Materials Research Express

PAPER

SnO_2 nanoparticles functionalized MoS_2 nanosheets as the electrode material for supercapacitor applications

Materials Research Express

PAPER

SnO_2 nanoparticles functionalized MoS_2 nanosheets as the electrode material for supercapacitor applications

RECEIVED
31 December 2018

REVISED
18 April 2019

ACCEPTED FOR PUBLICATION
16 May 2019

PUBLISHED
22 May 2019

C Prabukumar[1], M Mohamed Jaffer Sadiq[2], D Krishna Bhat[2] and K Udaya Bhat[1]

[1] Department of Metallurgical and Materials Engineering, National Institute of Technology Karnataka, Surathkal, Mangalore 575025, India

[2] Department of Chemistry, National Institute of Technology Karnataka, Surathkal, Mangalore 575025, India

E-mail: udayabhatk@gmail.com

Keywords: supercapacitor, MoS_2 nanosheets, SnO_2 nanoparticles, nanocomposite, ligand exchange process

Abstract

Tin oxide (SnO_2) nanoparticles undergo the volume expansion during an electrochemical cycle. This volume expansion leads to discontinuities in the form of microcracks in the electrode material. The problem of charge transportation associated with this microcracking limits the application of SnO_2 in the energy storage application such as supercapacitors. The present work approached to solve this problem by incorporating the MoS_2 nanosheets along with the SnO_2 nanoparticles. The SnO_2 nanoparticles are functionalized onto the surface of the MoS_2 nanosheets by the ligand exchange process. The MoS_2 nanosheets act as the support material for the SnO_2 nanoparticles. The electrode material prepared using SnO_2 nanoparticles and nanocomposite of SnO_2 functionalized MoS_2 nanosheets are tested by cyclic voltammetry and galvanostatic charge-discharge measurements. The specific capacity of the MoS_2–SnO_2 nanocomposite is calculated to be 61.6 F g^{-1} which is 4.4 fold higher than that of bare SnO_2 nanoparticles. The improvement in the electrochemical performance of SnO_2 is attributed to the high surface area and the charge transportation provided by the MoS_2 nanosheets.

1. Introduction

In recent years, most of the researches are focussed on to improve the performance of the energy generation and storage devices. The supercapacitors are being evolved as a promising energy storage device for the future. The supercapacitors possess some superior qualities than their peers, namely batteries. Unlike batteries, the charging and discharging process is faster for the supercapacitors. With the higher power density and longer life time than the batteries [1], the supercapacitors will play a major role in the field of energy storage in the coming years. Recently, the metals oxides (Sn, Mn, Ti, Co) are being explored for such applications [2–5]. Tin oxide (SnO_2) is a potential electrode material in energy storage applications, due to its low cost, high theoretical capacity and high electron mobility. However, there is a concern associated with the SnO_2 electrode that needs to be addressed. The volume expansion of the SnO_2 particles during the electrochemical process hinders the performance of the SnO_2 electrode [6]. Charge transfer in the SnO_2 electrode is affected due to the discontinuity caused by the volume expansion [7]. This results in reduction in the capacitance value of the SnO_2 electrode. To address this issue, the two-dimensional materials like graphene are used along with SnO_2 nanoparticles to facilitate charge transportation [8].

Molybdenum disulfide (MoS_2) is a material having fascinating properties, like, high surface area, higher ionic conductivity than metal oxides [9] and good mechanical flexibility [10]. It is widely used in gas sensors, supercapacitors, batteries, hydrogen evolution reactions and electronic applications [11–15]. The MoS_2 nanosheets are synthesised either by bottom-up approaches, such as hydrothermal, chemical vapour deposition (CVD) or by top-down approaches, like, ball milling, mechanical exfoliation and liquid phase exfoliation [12, 16–19]. Among them, liquid phase exfoliation is the simple and high yielding route to prepare the MoS_2 nanosheets. The solvents such as ethanol, dimethylformamide (DMF), N-Methyl-2-pyrrolidone (NMP) are

used to exfoliate the bulk MoS_2 particles into nanosheets [19, 20]. The MoS_2 nanosheets are proved to improve the electrochemical performance of materials like Co_3O_4, polyethylene dioxythiophene (PEDOT), polyaniline (PANI) and Mn_3O_4 [5, 21–23]. So, it is presumed that the electrochemical stability of the SnO_2 could be improved by using MoS_2 nanosheets along with the SnO_2 nanoparticles.

There are very limited studies reported focussing on the supercapacitor application with the combination of MoS_2–SnO_2 phases as nanocomposite [24]. The hydrothermal method is the widely used technique to prepare MoS_2–SnO_2 nanocomposite [25]. But it requires the temperature as high as 220 °C to produce nanosheets of MoS_2. In the present work, we have used a ligand exchange process to prepare MoS_2–SnO_2 nanocomposite. Here, the SnO_2 nanoparticles are functionalized on to the surface of the MoS_2 nanosheets at room temperature. The route is expected to be energy saving and producing the MoS_2–SnO_2 nanocomposite which will serve as a good supercapacitor electrode material.

2. Experimental details

2.1. Synthesis of MoS_2 nanosheets

The MoS_2 nanosheets were prepared by ultrasonication-assisted liquid phase exfoliation method [26]. All the chemicals are of analytical grade purchased from reputed manufacturers. Firstly, 150 mg of polyvinylpyrrolidone (PVP, MW $\sim$ 40,000) was dissolved in 10 ml ethanol. Then, 30 mg of bulk MoS_2 powder (Alfa Aesar, 325 mesh) was added into the prepared PVP solution. The mixture of MoS_2 and PVP in ethanol was ultrasonicated (Power $=$ 50 W, f $=$ 33 kHz) for 4 h to exfoliate MoS_2 nanosheets. After the exfoliation process, the exfoliated MoS_2 sheets which remained on top of the solution were transferred to the centrifugal tubes for washing. The product was mixed with acetone and centrifuged at 7000 rpm for 20 min. After removing the supernatant, isopropyl alcohol (IPA) was added to the precipitate. The product was again centrifuged at 8000 rpm for 20 min. Finally, the washed product was collected and suspended in IPA for storing.

2.2. Synthesis of SnO_2 nanoparticles

The SnO_2 nanoparticles were synthesised by following the work reported in the literature [27]. First, 1 g of tin chloride pentahydrate ($SnCl_4.5H_2O$) was dissolved in 10 ml of ethylene glycol (EG). It was followed by the addition of 250 mg of ammonium chloride, 250 mg of ammonium acetate and 30 ml de-mineralized (DM) water in a round bottom flask. Then, the flask was heated to 90 °C in the oil bath for 2 h. The synthesised product was washed by DM water and ethanol. Then it was dispersed in ethanol.

2.3. Functionalization of MoS_2 nanosheets with SnO_2 nanoparticles

The known density of MoS_2 nanosheets dispersion was added into a vial containing the known weight of SnO_2 nanoparticles dispersion. Then the two materials were well dispersed together by using ultrasonication bath. After the ultrasonication, the materials were allowed to get settled down at the bottom of the vial. Then the supernatant liquid was removed and the materials settled at the bottom were used for our study. Likewise, five different compositions of MoS_2–SnO_2 nanocomposites were prepared with varying the weight ratio of MoS_2 nanosheets (0.5%, 1%, 2.5%, 5% and 10%) to SnO_2 nanoparticles. The camera images of each step involved in this preparation process are shown in figure 1.

2.4. Materials characterization

The structural characterization and phase identification were performed by using x-ray diffractometer (XRD; JEOL, JDX 8) with Cu K_α ($\lambda = 0.154$ nm) radiation at the scan rate of 1° min^{-1}. The morphological features were studied by using field emission scanning electron microscope (FESEM; Carl Zeiss Sigma) and transmission electron microscope (TEM; JEOL, JEM-2100). The Raman spectra of bulk and exfoliated MoS_2 were obtained by using Raman spectrometer (Horiba Jobin-Yvon, labRAM HR) with an excitation wavelength of 532 nm. The surface chemistry of the materials was analysed by using x-ray photoelectron spectrometer (XPS; Thermo scientific, Multilab 2000) instrument (Mg Kα x-ray, 200 W as excitation source). The particle size of SnO_2 nanoparticles was determined by using particle size analyser (Malvern Zeta Sizer, NanoZS). The Specific surface area and pore size distribution were analysed by Brunauer–Emmett–Teller (BET) and Barrett–Joyner–Halenda (BJH) method using surface area analyser (Microtrac, BELSORP Max).

2.5. Electrochemical studies

Electrochemical studies were carried out with a standard three-electrode cell using SP-150 electrochemical workstation (BioLogic, France). Platinum wire and saturated calomel electrode (SCE) were used as the counter electrode and reference electrode, respectively. The working electrode was prepared as follows: 4.5 mg of nanocomposite was added into 250 μl water/ethanol (2:1 v/v) solution containing 15 μl Nafion (5 wt%). The

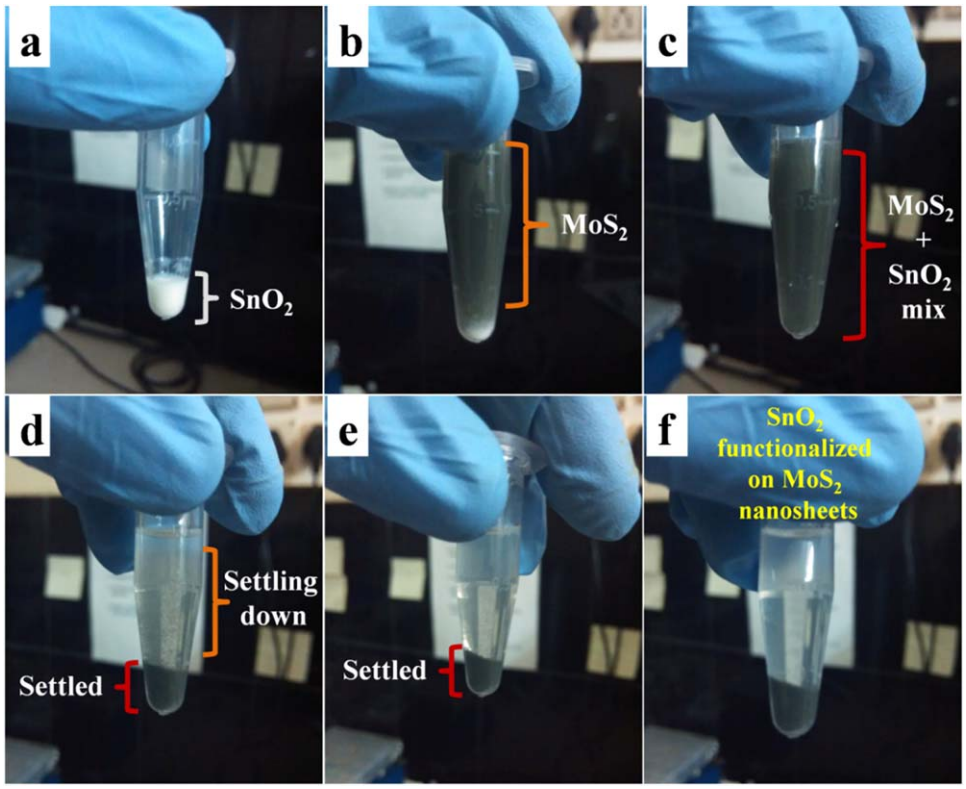

Figure 1. Camera images show the steps involved in the preparation of MoS_2–SnO_2 nanocomposite.

above mixture was ultrasonicated for 15 min to obtain a homogeneous mixture. 50 μl of the prepared mixture was drop cast on a graphite electrode (10 mm diameter rod). The calculated mass of the active electrode material was 1.1 mg cm^{-2}. The aqueous solution of 2 M KOH was used as the electrolyte.

3. Results and discussion

Figures 2(a), (b) show the FESEM micrographs of the bulk MoS_2 powder and exfoliated MoS_2 nanosheets. The bulk powder consisted of several layers of the MoS_2 stacked one above the other. The FESEM micrograph of exfoliated nanosheets revealed that the bulk MoS_2 powder was exfoliated into nanosheets. The synthesised SnO_2 nanoparticles (figure 2(c)) showed the spherical-like morphology with size in the range of 10–35 nm. Figure 2(d) shows the FESEM micrograph of the MoS_2–SnO_2 nanocomposite prepared by the ligand exchange process. The SnO_2 nanoparticles were functionalized over the surface of the MoS_2 nanosheets. The SnO_2 nanoparticles were firmly attached on to the surface of the MoS_2 nanosheets. Figure 3 shows the schematic diagram explaining the functionalization of MoS_2 nanosheets with SnO_2 nanoparticles by the ligand exchange process.

A thin layer of PVP molecules, from the exfoliation step, would still present onto the surface of the MoS_2 nanosheets even after washing process because of C-S and O-S bonding between PVP and MoS_2 [28]. Also, this PVP ligand attached with MoS_2 nanosheets kept nanosheets separated from each other. On the other hand, ammonium ions from ammonium salts during the synthesis process coordinated with the SnO_2 nanoparticles. These ammonium ions act as the surfactant to control the growth of the nanoparticles [27]. When the MoS_2 nanosheets and SnO_2 nanoparticles were mixed together (figures 1(b), (c)), the ammonium ions attached with the SnO_2 nanoparticles strip off the PVP molecules from the surface of the MoS_2 nanosheets. Subsequently, the vacant sites left by the stripped PVP molecules were occupied by SnO_2 nanoparticles. The ammonium ions present over the SnO_2 nanoparticles would help them to anchor onto the surface of the MoS_2 nanosheets [27]. Likewise, the SnO_2 nanoparticles were decorated or functionalized on the surface of the MoS_2 nanosheets. This functionalization process by exchanging the ligands is energy efficient compared to hydrothermal which involves high temperature and pressure [16].

Once the PVP molecules were replaced by SnO_2 nanoparticles from the MoS_2 surface, the MoS_2 nanosheets functionalized with SnO_2 nanoparticles were started to settle down as the precipitate (figures 1(e), (f)). The supernatant containing these PVP molecules was removed out and the obtained precipitate was used for our present studies.

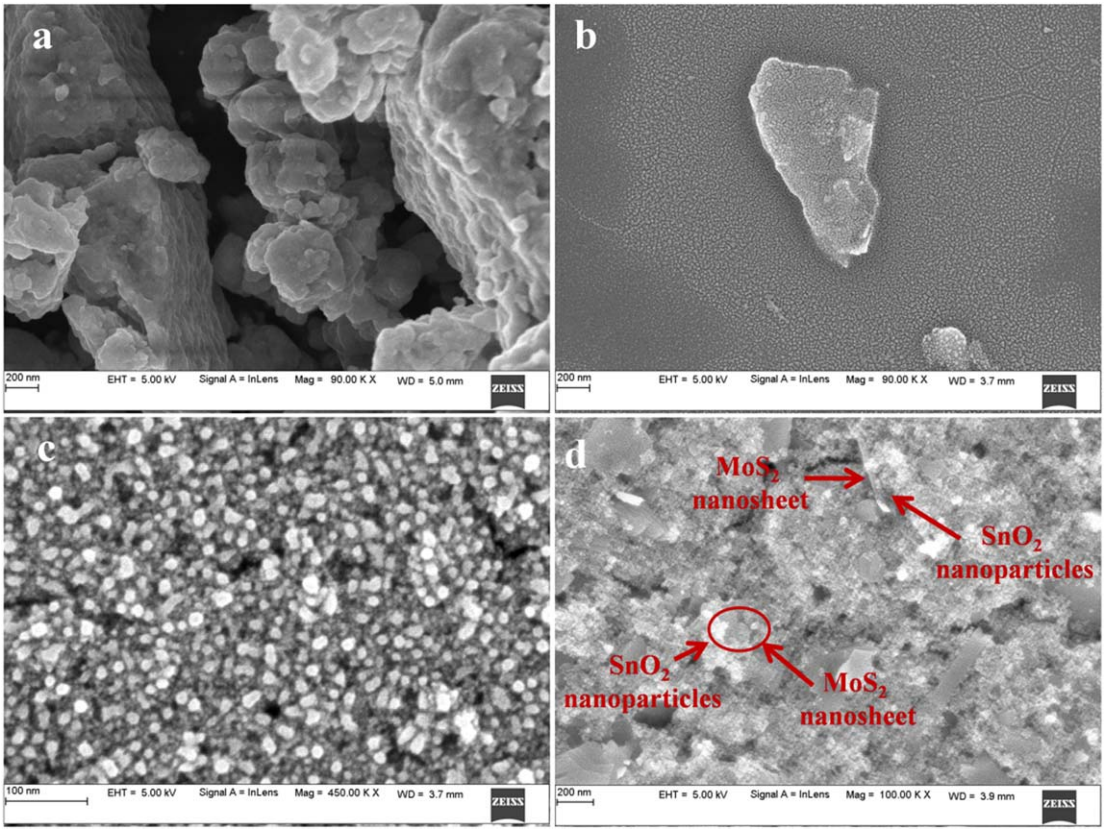

Figure 2. SEM micrograph of the (a) bulk MoS_2 powder, (b) exfoliated MoS_2 nanosheets, (c) synthesised SnO_2 nanoparticles, (d) MoS_2–SnO_2 nanocomposite.

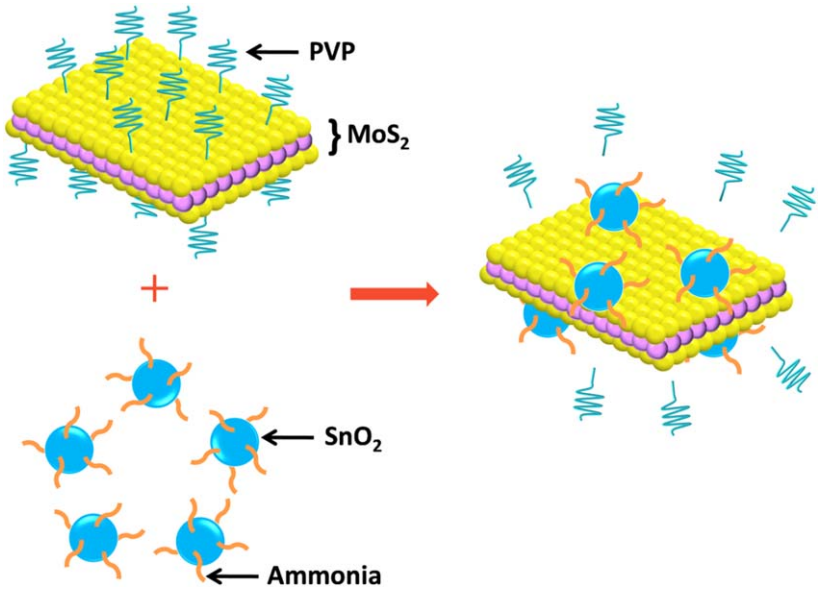

Figure 3. Schematic diagram explains the functionalization of MoS_2 nanosheets with SnO_2 nanoparticles.

Figure 4(a) shows the TEM micrograph of the exfoliated MoS_2 nanosheets. The exfoliated nanosheets contain only a few layers of MoS_2. The lattice distance of 0.27 nm is measured from the high-resolution TEM image shown in figure 4(b). It is attributed to (100) plane of MoS_2. The SAED pattern (inset figure 4(a)) revealed the hexagonal lattice structure of the MoS_2 nanosheets. The TEM micrograph of the synthesized SnO_2 nanoparticles showed in figure 4(c) affirmed the spherical-like morphology of the synthesised product. The lattice distances (interplanar spacing) in SnO_2 nanoparticles were measured to be 0.34 nm and 0.26 nm. These

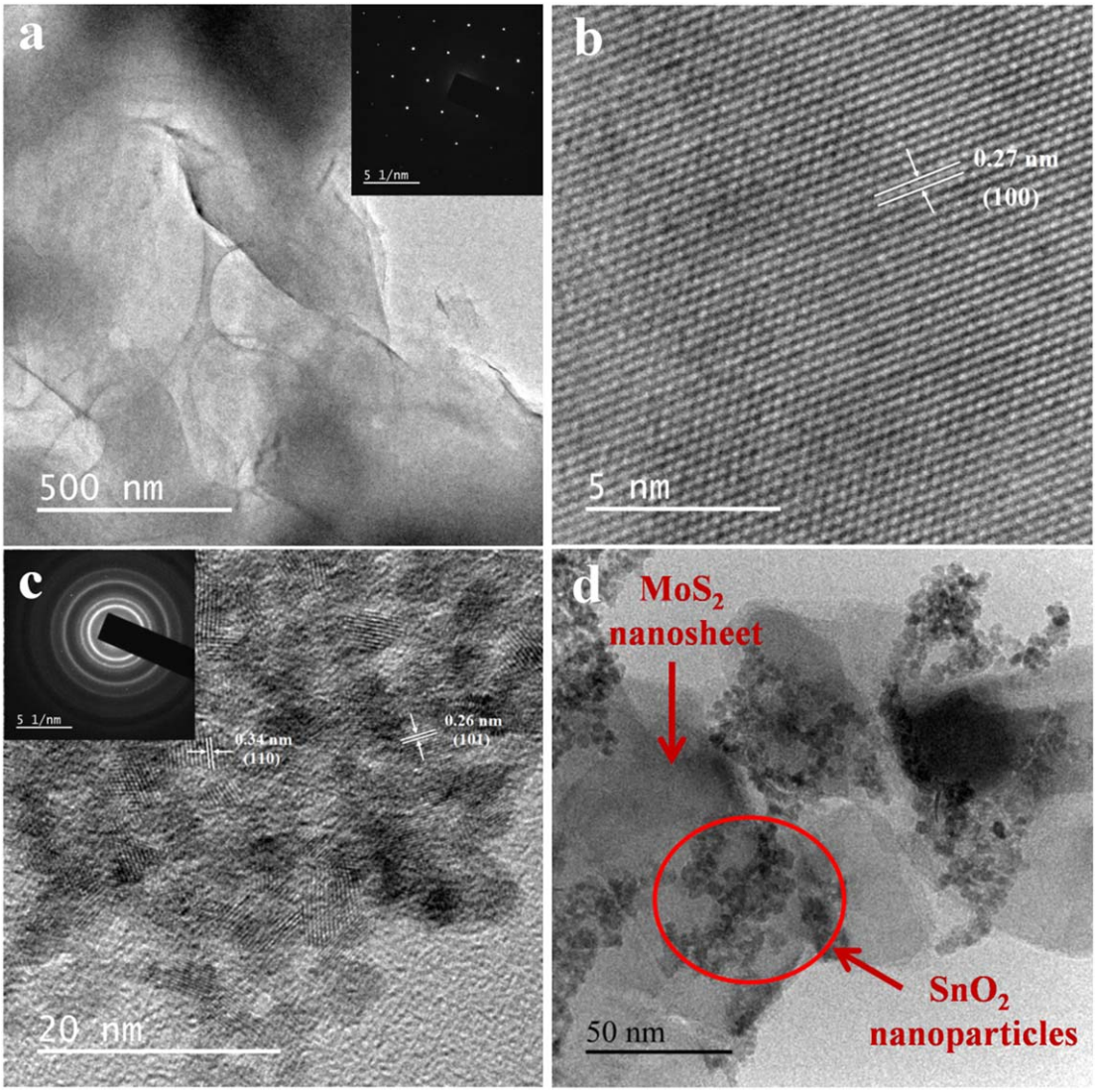

Figure 4. TEM micrograph of the (a) MoS_2 nanosheets (inset: SAED pattern), (b) Lattice image of the MoS_2 nanosheet, (c) SnO_2 nanoparticles (inset: SAED pattern), (d) MoS_2–SnO_2 nanocomposite.

values were well matched to (101) and (110) planes of the SnO_2, respectively. Figure 4(d) shows the TEM micrograph of the MoS_2–SnO_2 nanocomposite. The SnO_2 nanoparticles can be seen functionalized on the surface of the MoS_2 nanosheets.

The XRD patterns of bulk MoS_2 powder and exfoliated MoS_2 nanosheets are shown in figure 5(a). The XRD pattern of both materials belongs to the Molybdenite-2H phase (JCPDS #006-0097). The maximum intensity was observed for the peak belonged to (002) plane for both materials. But the peaks of (103) and (105) planes appeared for the bulk powder were absent for the exfoliated nanosheets. Also, the peak of (002) plane was broader for the exfoliated nanosheets compared to the bulk powder. This indicates the reduction in the thickness of the MoS_2 nanosheets after the exfoliation process. Figure 5(b) shows the XRD patterns of SnO_2 nanoparticles and MoS_2–SnO_2 nanocomposite along with MoS_2 nanosheets. Three peaks were observed at the angle of 26.2°, 33.8° and 51.2° for SnO_2 nanoparticles which are attributed to (110), (101) and (211) planes of SnO_2 (Cassiterite, JCPDS #041-1445). The XRD pattern of MoS_2–SnO_2 nanocomposite exhibited the peaks of both SnO_2 and MoS_2 phases.

The Raman spectra of bulk MoS_2 and MoS_2 nanosheets are shown in the figure 6. The characteristic Raman vibration peaks of E^1_{2g} and A_{1g} for bulk MoS_2 are observed at 383 cm^{-1} and 407 cm^{-1}, respectively [29]. When thickness of the MoS_2 sheet decreases, the E^1_{2g} peak belonging to in-plane sulfur-molybdenum vibration shifts to higher frequency, whereas, the A_{1g} peak belonging to out-plane sulphur vibration shifts to lower frequency [29]. The exfoliated MoS_2 nanosheets exhibited E^1_{2g} and A_{1g} peaks at 384 cm^{-1} and 405.5 cm^{-1}, respectively. The frequency gap between two Raman peaks of the exfoliated MoS_2 nanosheets was reduced to 21.5 cm^{-1} from 24 cm^{-1}. This is the indication that the bulk MoS_2 was exfoliated to nanosheets with few layers thickness [30].

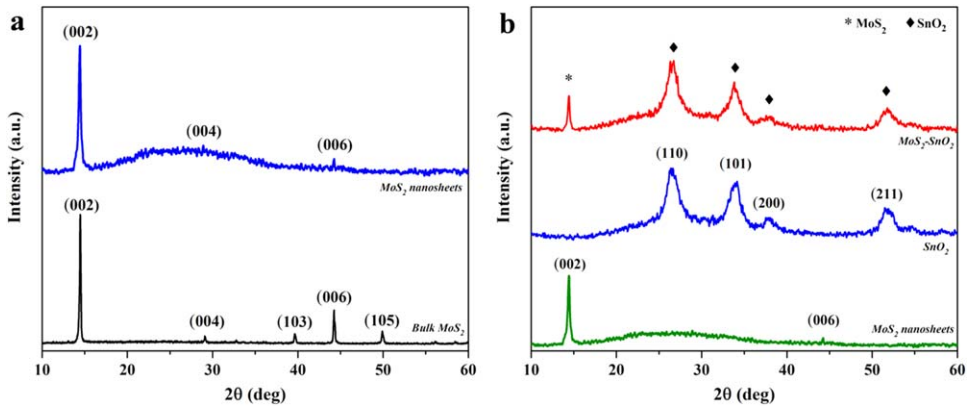

Figure 5. XRD pattern of (a) bulk MoS_2 powder and exfoliated MoS_2 nanosheets, (b) exfoliated MoS_2 nanosheets, SnO_2 nanoparticles and MoS_2–SnO_2 nanocomposite.

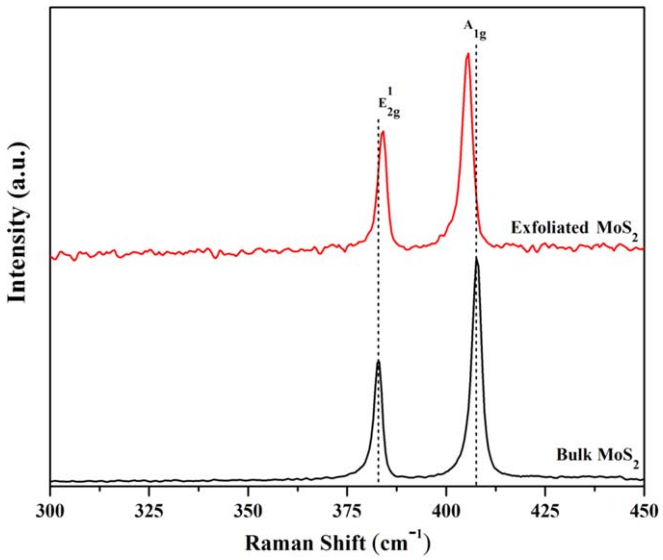

Figure 6. Raman spectrum of bulk MoS_2 powder and exfoliated MoS_2 nanosheets.

Figure 7(a) shows the particle size distribution chart of SnO_2 nanoparticles obtained from the particle analysis test. It is observed that the average size of the synthesised SnO_2 nanoparticles was calculated as 17.7 nm. Almost 90% of the particles fall in the size range of 10–21 nm with rest of the particles fall in the size range of 25–37 nm. Figure 7(b) shows the Nitrogen adsorption-desorption curve and pore size distribution (Inset) of the MoS_2 nanosheets. The adsorption-desorption isotherm with a small hysteresis loop indicates that the isotherm is a type IV isotherm as defined by the IUPAC [31]. The pore size distribution curve shows the peaks at the pore size of 6.2 nm, 8.2 nm and 14 nm with the mean pore size of 7.7 nm. This indicates the mesoporous nature of the dried MoS_2 nanosheets powder [31]. The specific surface area (S_a) of the MoS_2 nanosheets measured by BET method was 17.5 $m^2\ g^{-1}$. This S_a value of MoS_2 nanosheets was marginally larger than the previously reported values [31, 32].

In the XPS survey spectrum of MoS_2–SnO_2 nanocomposite (figure 8(a)), the presence of peaks corresponding to Mo, Sn, S, O, N and C elements were observed. The high-resolution XPS spectrum of Mo 3d region (figure 8(b)) exhibited two peaks at binding energies 229.4 and 232.4 eV belonged to $3d_{5/2}$ and $3d_{3/2}$, respectively. These binding energies were corresponding to the +4 oxidation state of Mo. Also, a broad peak corresponding to S 2 s was observed at 226.5 eV in the same spectrum. The high-resolution XPS spectrum of Sn 3d region is shown in figure 8(c). Two peaks at 487.4 and 495.8 eV were observed. These were belonged to $3d_{5/2}$ and $3d_{3/2}$ of Sn (+4 oxidation state), respectively. The XPS spectrum of S is shown in figure 8(d). The XPS spectrum of S 2 s region was resolved into a doublet peak, with the binding energies 162.2 and 163.2 eV corresponding to $2p_{3/2}$ and $2p_{1/2}$ of S, respectively. The above results confirm the presence of MoS_2 and SnO_2 without any other oxidation products [25].

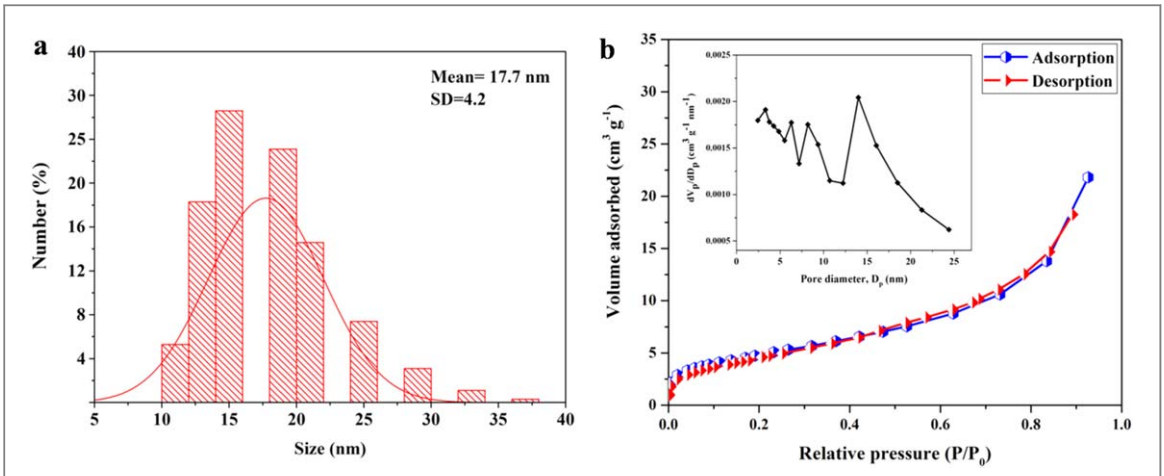

Figure 7. (a) Particle size distribution of SnO_2 nanoparticles, (b) Nitrogen adsorption-desorption curve of MoS_2 nanosheets; Inset: Pore size distribution.

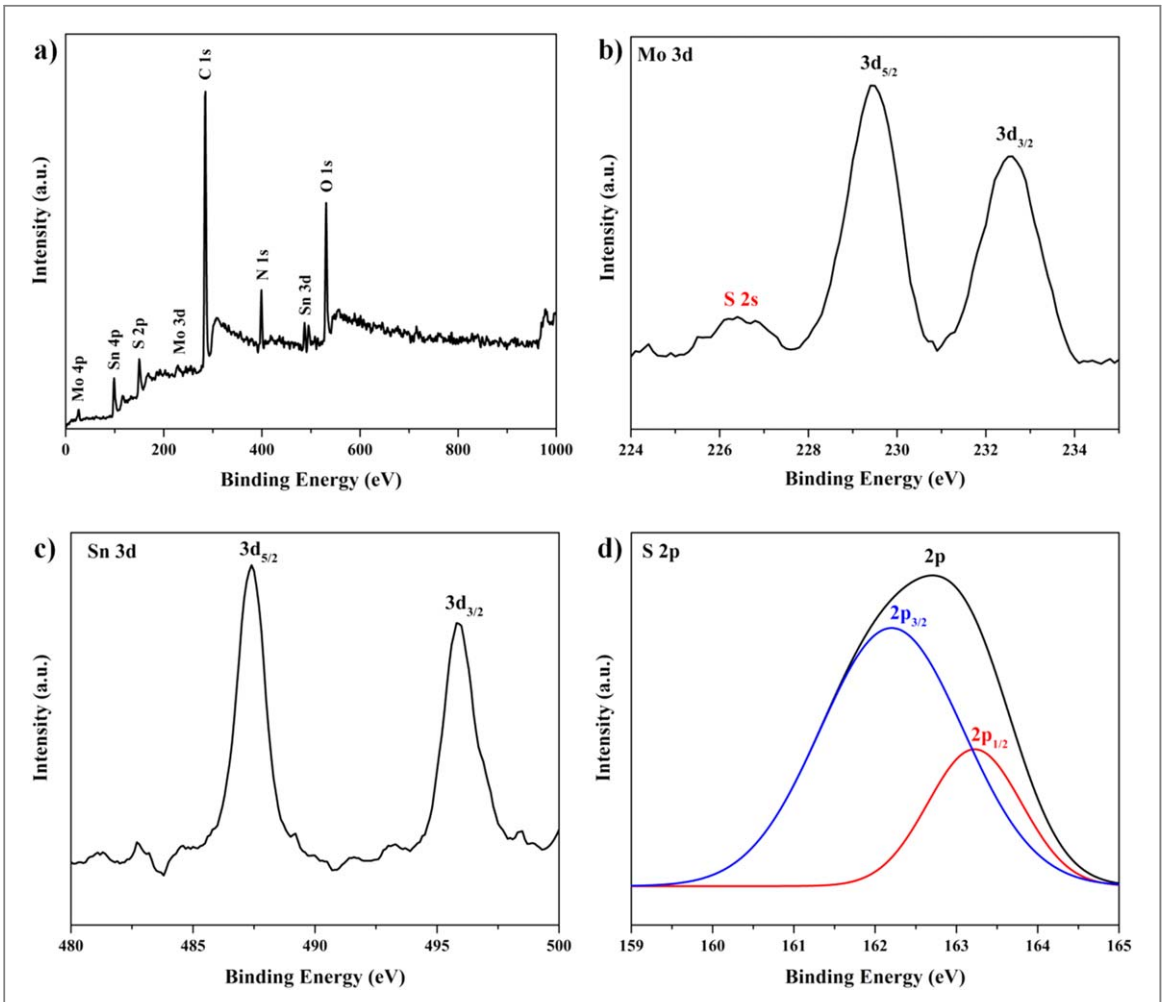

Figure 8. (a) XPS spectrum of MoS_2–SnO_2 nanocomposite, high resolution XPS spectrum of (b) Mo 3d, (c) Sn 3d, (d) S 2p.

The cyclic voltammetry (CV) was performed for SnO_2 and MoS_2–SnO_2 between the potential value range of −0.2 V to 0.8 V. The CV plots are showed in figure 9(a). CV curves for all samples showed the double layer supercapacitor behavior with semi rectangular shape curve. This result was in accordance with the previously reported results [2, 12]. From figure 9(a), it was observed that the output current density of the MoS_2–SnO_2 nanocomposite is higher than the output current density of the bare SnO_2 nanoparticles. During the electrochemical process the SnO_2 nanoparticles undergo the volume expansion that lead to increase in the

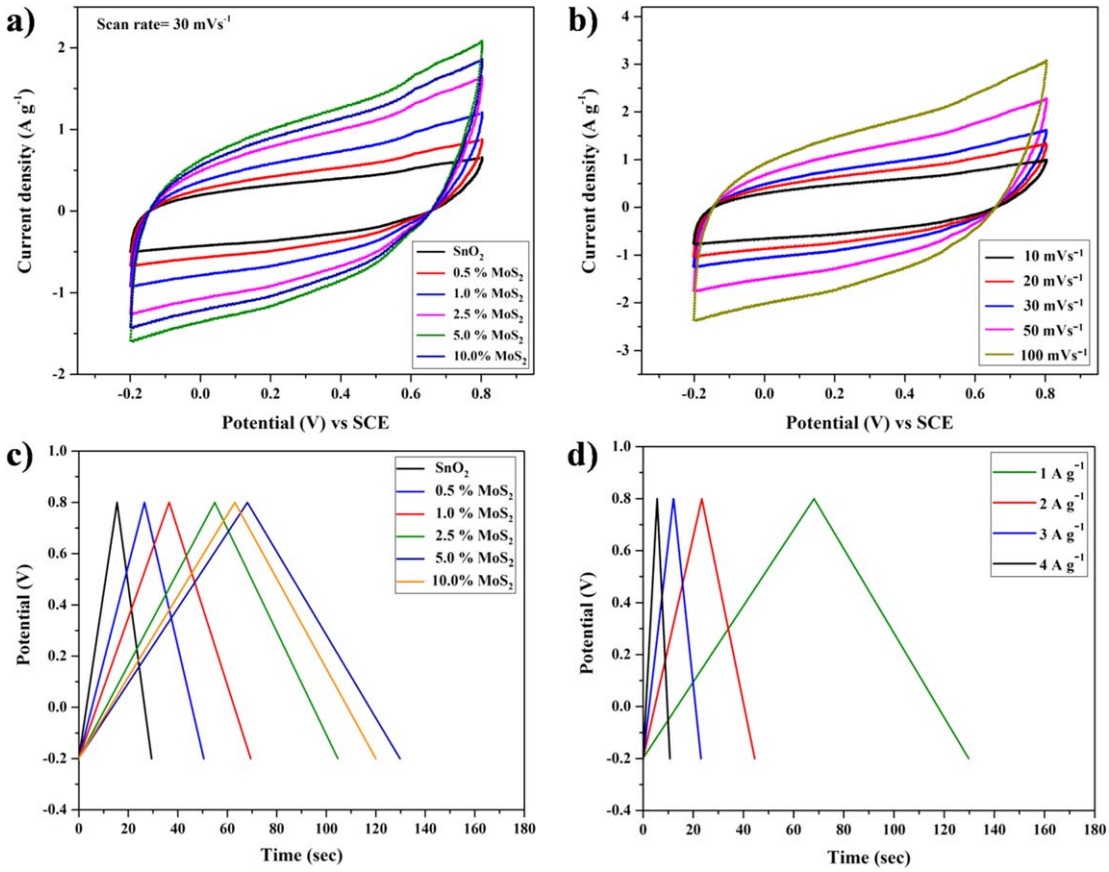

Figure 9. Cyclic voltammetric curves of (a) bare SnO_2 nanoparticles and MoS_2–SnO_2 nanocomposite at scanning speed of 30 mV s^{-1}, (b) 5% MoS_2–SnO_2 at different scanning speeds, between applied potential range of −0.2 V to 0.8 V, (c) Galvanostatic charge-discharge curves of the SnO_2 and the MoS_2–SnO_2 at constant current density of 1 A g^{-1}, (d) Charge-discharge curves of 5% MoS_2–SnO_2 at different current values.

particle size. The increase in the particle size leads to microcracks between the SnO_2 particles [6, 7]. The formation microcracks and reduction in the surface area were the reasons for the low performance of the SnO_2 nanoparticles. Addition of the MoS_2 nanosheets bridged the SnO_2 nanoparticles and provided the high surface area for the ion transportation between electrode and electrolyte. So, a gradual increase in the output current was observed with respect to increase in the MoS_2 to SnO_2 ratio. The 5% MoS_2–SnO_2 nanocomposite exhibited the highest current density amongst all the electrode materials. But the current density started to decrease when the MoS_2 ratio was increased to 10%. So it is concluded that the 5% is the optimum MoS_2–SnO_2 ratio for the supercapacitor application. Figure 9(b) shows the CV curves of 5% the MoS_2–SnO_2 nanocomposite at scanning speeds of 10, 20, 30, 50 and 100 mVs^{-1} respectively. The obtained CV curves for all the scanning speeds are showing semi rectangular curve corresponding to double layer capacitance.

Figure 9(c) shows the galvanostatic charge-discharge curve of the SnO_2 and the MoS_2–SnO_2 nanocomposite. The charge-discharge study was performed within the potential of −0.2 V to 0.8 V at an applied current of 1 A g^{-1}. The obtained charge-discharge curves are linear and triangular in shape. This indicated the capacitance nature of the used electrode materials. The discharge time of the SnO_2 nanoparticles was 14 s, whereas, the MoS_2–SnO_2 nanocomposite showed longer discharge time. The discharge time was increased from 24 s for 0.5% MoS_2–SnO_2 to 61 s for 5% MoS_2–SnO_2.

As mentioned earlier, the SnO_2 particles would go through volume or size change during the electrochemical process [6, 7]. This would lead to microcracks in the SnO_2 electrode. The discontinuities formed by this cracks would affect the charge transportation. But, when the MoS_2 nanosheets were introduced with the SnO_2 nanoparticles, the nanosheets acted as a conductive pathway between the SnO_2 nanoparticles. This is explained schematically in figure 10. The MoS_2 nanosheets would anchor the SnO_2 nanoparticles within its surface and bridge the neighboring SnO_2 nanoparticles, electrically to help the charge transfer easier during the charge-discharge process [22]. The large surface area of MoS_2 nanosheets leads to effective interaction between the electrode and the electrolyte. Thus, the electrochemical performance (CV curve area and discharge time) was increased for the MoS_2–SnO_2 nanocomposite. But, it was noticed that the increasing the MoS_2 ratio beyond 5% the discharge time started to decrease. When the ratio of the MoS_2 was increased above the optimum value, the

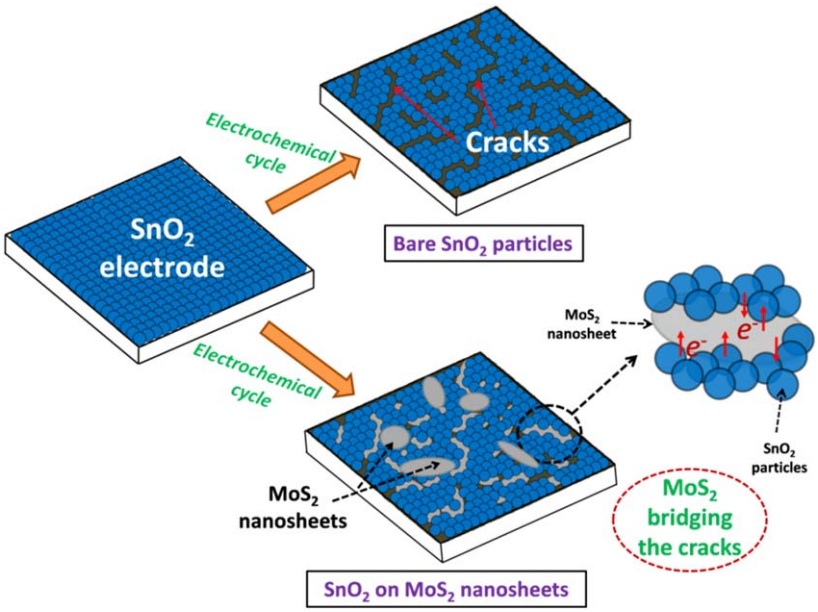

Figure 10. Schematic representation of the microcracks in the SnO_2 electrode and MoS_2 nanosheets bridging the microcracks.

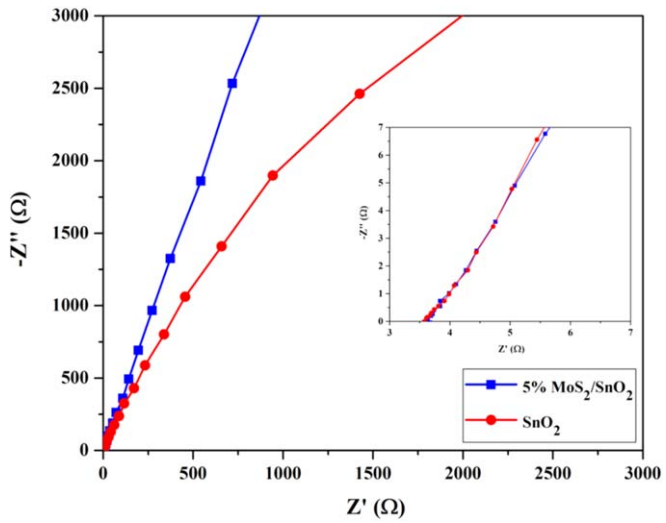

Figure 11. Nyquist curve of SnO_2 and 5% MoS_2–SnO_2 nanocomposite (Inset: Plot is magnified at high frequency region).

discharge time started to decrease because of the reduction in active SnO_2 material. So it is concluded that the 5% is the optimum ratio in the MoS_2–SnO_2 nanocomposite. This is also in accordance with the cyclic voltammetry study.

The Nyquist plot obtained from the electrochemical impedance spectroscopy (EIS) is shown in figure 11. EIS was performed over the frequency range of 0.1 Hz to 100 kHz for bare SnO_2 and 5% MoS_2–SnO_2 are compared. A straight line was observed for both materials at lower frequency region. However, the slope of 5% MoS_2–SnO_2 nanocomposite was higher than that of the bare SnO_2 nanoparticles. This proves that the electronic resistance of the MoS_2–SnO_2 nanocomposite was lower than that of the bare SnO_2 nanoparticles. It indicated that the MoS_2–SnO_2 nanocomposite exhibited more ideal capacitor behavior than the bare SnO_2 nanoparticles. The high-frequency region was enlarged and shown as inset image. The curves tend to show a very small loop, the characteristics of charge transfer resistance, at higher frequency region. It is attributed to low charge transfer resistance of the electrode [33]. The solution resistance is the value at which the curve is intersecting with real axis. The values were almost equal for 5% MoS_2–SnO_2 nanocomposite and SnO_2 nanoparticles with 3.67 and 3.6 Ω respectively.

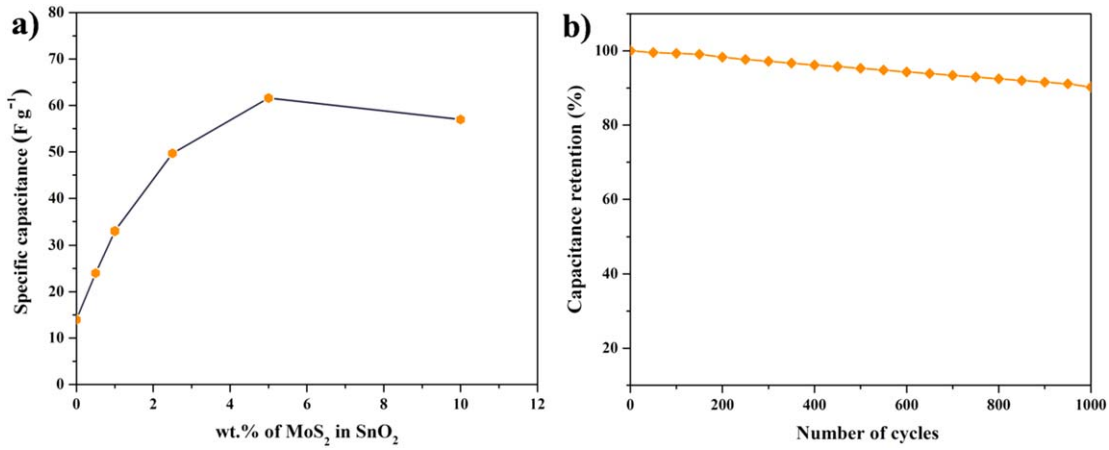

Figure 12. (a) Specific capacitance of the MoS_2–SnO_2 nanocomposites with different ratio of MoS_2 in the composite, (b) Capacitance retention versus number of cycles for the 5% MoS_2–SnO_2 nanocomposite.

The specific capacitance was calculated from the charge-discharge curve by the following equation [22],

$$C_s = (I \,.\, t_d)/(m \,.\, \Delta V) \quad (1)$$

where, 'C_s' is the specific capacitance (F g^{-1}), 'I' is the discharge current (A), 't_d' is the discharge time (s), 'm' is the mass of the electrode material (g) and 'ΔV' is the potential window. The values of C_s for SnO_2 and MoS_2–SnO_2 were plotted and shown in figure 12(a).

The specific capacitance (C_s) of bare SnO_2 nanoparticles was calculated to be 14 F g^{-1}. The specific capacitance value of the SnO_2 was increased after the addition of the MoS_2 nanosheets. The high surface area and easy the charge transportation between the electrode material and electrolyte were the reason for the increased vaue of specific capacitance. The 5% MoS_2–SnO_2 nanocomposite showed the highest specific capacitance value of 61.6 F g^{-1} which is 4.4 times greater than that of bare SnO_2 nanoparticles.

The capacitance retention curve of 5% MoS_2–SnO_2 over the charge-discharge of 1000 cycles is shown in figure 12(b). The MoS_2–SnO_2 showed very good cyclic stability by retaining 90% of its original capacitance even after 1000 number of charge-discharge cycles. This indicates that the electrochemical performance of the SnO_2 nanoparticles is improved by the addition of the MoS_2 nanosheets with the SnO_2. The reasons for the improvement in the performance are, (1) The MoS_2 nanosheets provided good support and conductive path in the electrode material when the microcracks are formed due to volume expansion of SnO_2; (2) The high surface area offered to the electrode in the form of nanosheets made it easier for the ion transportation between electrolyte and electrode.

4. Conclusions

The MoS_2–SnO_2 nanocomposite was prepared by functionalization of SnO_2 nanoparticles onto the surface of the MoS_2 nanosheets by ligand exchange process. The specific capacitance of the bare SnO_2 nanoparticles calculated from galvanostatic charge-discharge was 14 F g^{-1}. The low specific capacity of SnO_2 was due to the discontinuity in the electrode material caused by the formation of microcracks. The problem of microcracks was solved by incorporating SnO_2 nanoparticles on the surface of the MoS_2 nanosheets. The MoS_2 nanosheets acted as a conducting bridge between the SnO_2 nanoparticles to help in charge transportation during the charge-discharge process. Also the nanosheets provided helped to improve the interaction between the electrolyte and electrode material. Thus, the specific capacitance of the MoS_2–SnO_2 nanocomposite was increased to 61.6 F g^{-1}. By improving the electrochemical performance of SnO_2, the prepared MoS_2–SnO_2 nanocomposite paves a way to develop low-cost energy storage devices for the future.

Acknowledgments

Prabukumar would like to thank NIT Karnataka for providing financial support in the form of Institute fellowship. The author is very thankful to Dr Shashi Bhusan Arya, Assistant Professor, Dept. of MME, NITK for

providing the facility to carry out the electrochemical characterization. The author wants to thank Mr Prashant Huilgol, Research Scholar, Dept. of MME, NITK for helping in TEM images.

ORCID iDs

C Prabukumar https://orcid.org/0000-0002-5527-6974
M Mohamed Jaffer Sadiq https://orcid.org/0000-0001-5699-3038
D Krishna Bhat https://orcid.org/0000-0003-0383-6017
K Udaya Bhat https://orcid.org/0000-0002-0752-3600

References

[1] Choi J H, Lee C, Cho S, Moon G D, Kim B S, Chang H and Jang H D 2018 High capacitance and energy density supercapacitor based on biomass-derived activated carbons with reduced graphene oxide binder *Carbon* **132** 16–24
[2] Bonu V, Gupta B, Chandra S, Das A, Dhara S and Tyagi A K 2016 Electrochemical supercapacitor performance of SnO_2 quantum dots *Electrochim. Acta* **203** 230–7
[3] Aravinda L S, Udaya Bhat K and Bhat B R 2013 Porous MnO_2 nano whiskers bunch/activated carbon based composite electrodes for high energy density supercapacitor *ECS Solid State Lett.* **2** M61–3
[4] Aravinda L S, Nagaraja K K, Nagaraja H S, Bhat K U and Bhat B R 2016 Fabrication and performance evaluation of hybrid supercapacitor electrodes based on carbon nanotubes and sputtered TiO_2 *Nanotechnology* **27** 1–10
[5] Liang D, Tian Z, Liu J, Ye Y, Wu S, Cai Y and Liang C 2015 MoS_2 nanosheets decorated with ultrafine Co_3O_4 nanoparticles for high-performance electrochemical capacitors *Electrochim. Acta* **182** 376–82
[6] Lou X W, Wang Y, Yuan C, Lee J Y and Archer L A 2006 Template-free synthesis of SnO_2 hollow nanostructures with high lithium storage capacity *Adv. Mater.* **18** 2325–9
[7] Brousse T, Retoux R, Herterich U and Schleich D M 1998 Thin-film crystalline SnO_2-lithium electrodes *J. Electrochem. Soc.* **145** 373–87
[8] Dhanabalan A, Li X, Agrawal R, Chen C and Wang C 2013 Fabrication and characterization of SnO_2/Graphene composites as high capacity anodes for Li-Ion batteries *Nanomaterials* **3** 606–14
[9] Zheng N, Bu X and Feng P 2003 Synthetic design of crystalline inorganic chalcogenides exhibiting fast-ion conductivity *Nature* **426** 428–32
[10] Chhowalla M, Shin H S, Eda G, Li L J, Loh K P and Zhang H 2013 The chemistry of two-dimensional layered transition metal nanosheets *Nat. Chem.* **5** 263–75
[11] Cui S, Wen Z, Huang X, Chang J and Chen J 2015 Stabilizing MoS_2 nanosheets through SnO_2 nanocrystal decoration for high-performance gas sensing in air *Small* **11** 2305–13
[12] Krishnamoorthy K, Pazhamalai P, Veerasubramani G K and Kim S J 2016 Mechanically delaminated few layered MoS_2 nanosheets based high performance wire type solid-state symmetric supercapacitors *J. Power Sources* **321** 112–9
[13] Yang T, Chen Y, Qu B, Mei L, Lei D, Zhang H, Li Q and Wang T 2014 Construction of 3D flower-like MoS_2 spheres with nanosheets as anode materials for high-performance lithium ion batteries *Electrochim. Acta* **115** 165–9
[14] Chang K, Hai X, Pang H, Zhang H, Shi L, Liu G, Liu H, Zhao G, Li M and Ye J 2016 Targeted synthesis of 2H- and 1T-Phase MoS_2 monolayers for catalytic hydrogen evolution *Adv. Mater.* **28** 10033–41
[15] Bessonov A A, Kirikova M N, Petukhov D I, Allen M, Ryhänen T and Bailey M J A 2014 Layered memristive and memcapacitive switches for printable electronics *Nat. Mater.* **14** 199–204
[16] Ren X, Pang L, Zhang Y, Ren X, Fan H and Liu (Frank) S 2015 One-step hydrothermal synthesis of monolayer MoS_2 quantum dots for highly efficient electrocatalytic hydrogen evolution *J. Mater. Chem.* A **3** 10693–7
[17] Yu Y, Li C, Liu Y, Su L, Zhang Y and Cao L 2013 Controlled scalable synthesis of uniform, high-quality monolayer and few-layer MoS_2 films *Sci. Rep.* **3** 1866
[18] Kwon J, Hong Y K, Kwon H J, Park Y J, Yoo B, Kim J, Grigoropoulos C P, Oh M S and Kim S 2015 Optically transparent thin-film transistors based on 2D multilayer MoS_2 and indium zinc oxide electrodes *Nanotechnology* **26** 035202
[19] Weng Q, Wang X, Wang X, Zhang C, Jiang X, Bando Y and Golberg D 2015 Supercapacitive energy storage performance of molybdenum disulfide nanosheets wrapped with microporous carbons *J. Mater. Chem. A Mater. Energy Sustain.* **3** 3097–102
[20] Ghasemi F and Mohajerzadeh S 2016 Sequential solvent exchange method for controlled exfoliation of MoS_2 suitable for phototransistor fabrication *ACS Appl. Mater. Interfaces* **8** 31179–91
[21] Alamro T and Ram M K 2017 Polyethylenedioxythiophene and molybdenum disulfide nanocomposite electrodes for supercapacitor applications *Electrochim. Acta* **235** 623–31
[22] Huang K J, Wang L, Liu Y J, Wang H B, Liu Y M and Wang L L 2013 Synthesis of polyaniline/2-dimensional graphene analog MoS_2 composites for high-performance supercapacitor *Electrochim. Acta* **109** 587–94
[23] Wang M, Fei H, Zhang P and Yin L 2016 Hierarchically layered MoS_2/Mn_3O_4 hybrid architectures for electrochemical supercapacitors with enhanced performance *Electrochim. Acta* **209** 389–98
[24] Ma L, Zhou X, Xu L, Xu X and Zhang L 2016 Microwave-assisted hydrothermal preparation of SnO_2/MoS_2 composites and their electrochemical performance *Nano* **11** 16–8
[25] Chen Y, Lu J, Wen S, Lu L and Xue J 2014 Synthesis of SnO_2/MoS_2composites with different component ratios and their applications as lithium ion battery anodes *J. Mater. Chem.* A **2** 17857–66
[26] Liu J, Zeng Z, Cao X, Lu G, Wang L H, Fan Q L, Huang W and Zhang H 2012 Preparation of MoS_2-polyvinylpyrrolidone nanocomposites for flexible nonvolatile rewritable memory devices with reduced graphene oxide electrodes *Small* **8** 3517–22
[27] Bob B, Machness A, Song T B, Zhou H, Chung C H and Yang Y 2016 Silver nanowires with semiconducting ligands for low-temperature transparent conductors *Nano Res.* **9** 392–400
[28] Liu X, Wang T, Hu G, Xu C, Xiong Y and Wang Y 2018 Controllable synthesis of self-assembled MoS_2 hollow spheres for photocatalytic application *J. Mater. Sci., Mater. Electron.* **29** 753–61
[29] Rao R, Islam A E, Campbell P M, Vogel E M and Maruyama B 2017 *In situ* thermal oxidation kinetics in few layer MoS_2 *2D Mater.* **4** 25058

[30] Tsai M L, Su S H, Chang J K, Tsai D S, Chen C H, Wu C I, Li L J, Chen L J and He J H 2014 Monolayer MoS_2 heterojunction solar cells *ACS Nano* **8** 8317–22
[31] Fan L Q, Liu G J, Zhang C Y, Wu J H and Wei Y L 2015 Facile one-step hydrothermal preparation of molybdenum disulfide/carbon composite for use in supercapacitor *Int. J. Hydrog. Energy* **40** 10150–7
[32] Qiao X Q, Hu F-C, Tian F-Y, Hou D-F and Li D S 2016 Equilibrium and kinetic studies on MB adsorption by ultrathin 2D MoS_2 nanosheets *RSC Adv.* **6** 11631–6
[33] Sreejesh M, Huang N M and Nagaraja H S 2015 Solar exfoliated graphene and its application in supercapacitors and electrochemical H_2O_2 sensing *Electrochim. Acta* **160** 94–9